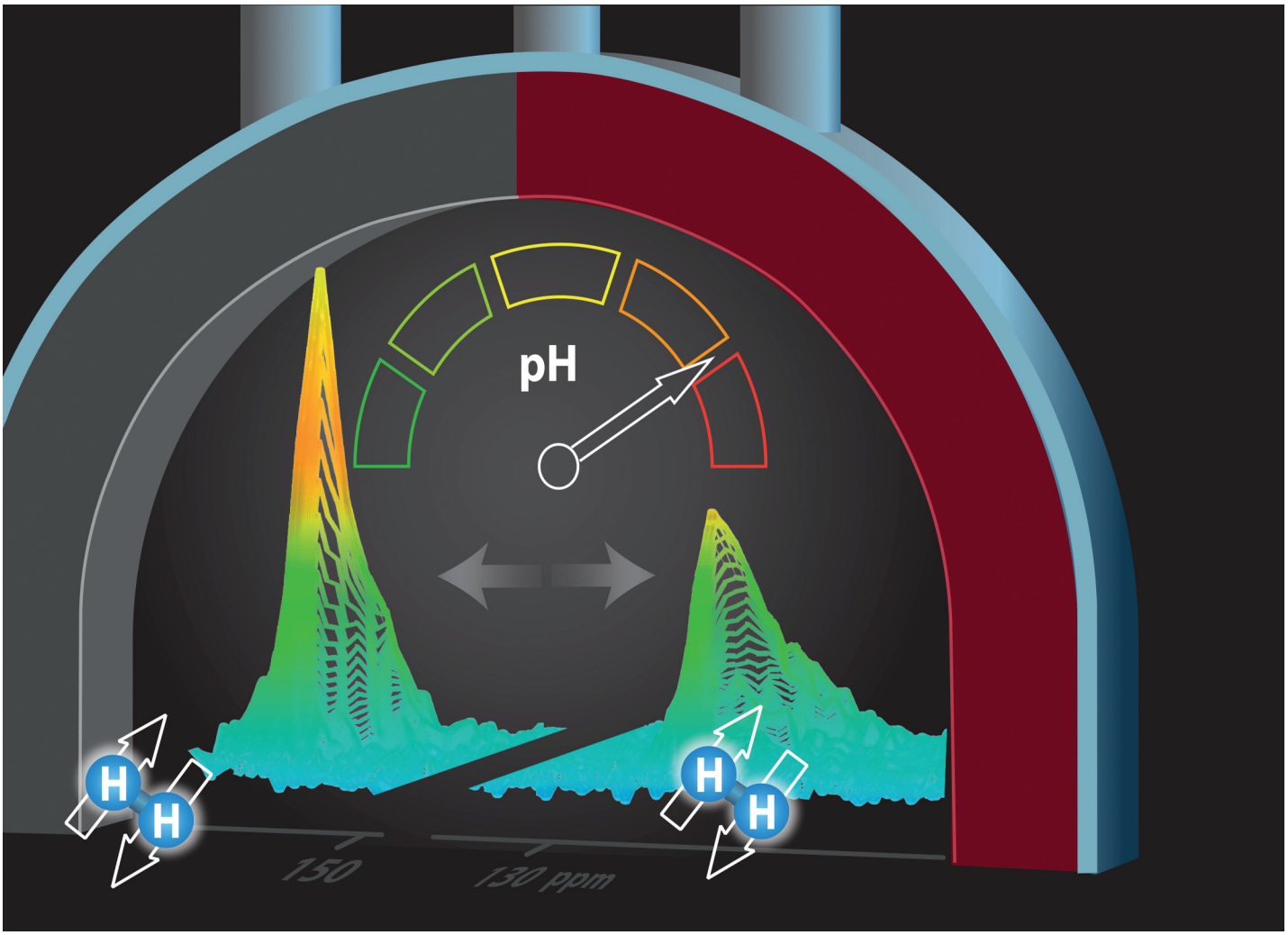

Showcasing research from Dr. Stefan Glöggler's team, NMR Signal Enhancement Group, Max Planck for Multidisciplinary Sciences, Göttingen, Germany.

Parahydrogen-enhanced pH measurements using [1-^{13}C] bicarbonate derived from non-enzymatic decarboxylation of [1-^{13}C]pyruvate-d_3

Non-invasive magnetic resonance methods to measure pH offer a new approach for early diagnosis of diseases characterized by acid–base imbalances. We present an optimized preparation of an hyperpolarized $H^{13}CO_3^-/^{13}CO_2$ pH sensor *via* non-enzymatic decarboxylation with H_2O_2 of [1-^{13}C]pyruvate-d_3. Unprecedented degrees of ^{13}C signal-enhancements of purified [1-^{13}C]pyruvate-d_3 were obtained using parahydrogen allowing for a secondary reaction to release the pH sensor. *In vitro* validations demonstrated accurate pH calculations. Our results highlight the efficiency of a pH sensor generated in less than one minute, with remarkable polarization, and biocompatibility suitable for future *in vivo* studies.

As featured in:

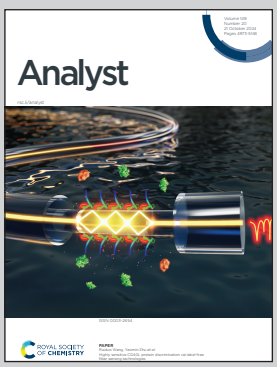

See Stefan Glöggler *et al.*, *Analyst*, 2024, **149**, 5022. Image designed and illustrated by Hartmut Sebesse, MPINAT MediaService

ROYAL SOCIETY OF CHEMISTRY

rsc.li/analyst

Registered charity number: 207890

Analyst

ROYAL SOCIETY OF CHEMISTRY

PAPER

View Article Online
View Journal | View Issue

Cite this: *Analyst*, 2024, **149**, 5022

Parahydrogen-enhanced pH measurements using [1-^{13}C]bicarbonate derived from non-enzymatic decarboxylation of [1-^{13}C]pyruvate-d$_3$†

Maria Daniela Santi, [a,b] Theresa Luca Katrin Hune,[a,b] Gonzalo Gabriel Rodriguez,[a,b] Lisa M. Fries,[a,b] Ruhuai Mei, [a,b] Sonja Sternkopf,[a,b] Josef Elsaßer[a,b] and Stefan Glöggler *[a,b]

Alterations in pH are a hallmark in several pathologies including cancer, ischemia, and inflammation. Non-invasive magnetic resonance methods to measure pH offer a new approach for early diagnosis of diseases characterized by acid–base imbalances. The hyperpolarization with parahydrogen-induced polarization (PHIP) enhances inherently low signals in magnetic resonance experiments by several orders of magnitude and offers a suitable platform to obtain biocompatible markers in less than one minute. Here, we present an optimized preparation of an hyperpolarized $H^{13}CO_3^-/^{13}CO_2$ pH sensor *via* non-enzymatic decarboxylation with H_2O_2 of [1-^{13}C]pyruvate-d$_3$ obtained by PHIP at 7 T. An improved ^{13}C polarization of purified [1-^{13}C]pyruvate-d$_3$ in water with 36.65 ± 0.06% polarization was obtained starting from 50 mM precursor. Subsequent decarboxylation, $H^{13}CO_3^-/^{13}CO_2$ exhibited 12.46 ± 0.01% of polarization at physiological pH, 45 seconds after the reaction start. Considering the dilution factor that [1-^{13}C]pyruvate-d$_3$ exhibits *in vivo*, we optimized our methodology to test the accuracy of the pH sensor at single digit millimolar concentration. *In vitro* pH estimations on phantoms and cell culture media demonstrated accurate pH calculations with uncertainties of less than 0.08 units. These promising results highlight the efficiency of a pH sensor generated *via* PHIP in less than one minute, with remarkable polarization, and biocompatibility suitable for future *in vivo* studies.

Received 12th June 2024,
Accepted 15th August 2024

DOI: 10.1039/d4an00832d

rsc.li/analyst

Introduction

pH is robustly regulated in healthy tissues and is essential for physiological processes including tissue oxygenation, proper protein structure, and various biochemical reactions.[1] However, perturbations of acid–base homeostasis are a common feature of several pathological conditions including cancer, ischemia, inflammation, renal disease, and infectious diseases.[2–4] It is known that the acidic microenvironment generated by cancer cells correlates with aggressiveness, migration, invasion, and metastasis potential.[5–7] All these events are associated with the Warburg effect, which involves increased glucose uptakes, anaerobic glycolysis, increased production of lactate, and an acidic extracellular pH.[8] Moreover, it was reported that aberrant acidifications could contribute to Alzheimer's disease and Amyotrophic lateral sclerosis' development.[9–11] Therefore, the development of safe and rapid pH measurement may aid in the early diagnosis of acid–base imbalances and subsequent pathological disorders. Although different techniques such as magnetic resonance spectroscopy (MRS), magnetic resonance imaging (MRI), and positron emission tomography (PET) have been used to measure pH in preclinical environments, none of them was successfully translated to routine clinical use.[4,12–22] Regarding MRS, ^{31}P and ^{19}F probes were used to measure pH *in vivo*. However, they present small pH dependent chemical shifts and lack of sensitivity.[13,23–27] Concerning MRI focused techniques, several methods were developed (*e.g.* CEST and the use of Gd^{3+}).[27,28] Overall, the main reasons why the noninvasive developed probes are challenging to be clinically translatable are centered on, (i) the potential toxicity of the existing probes which makes them unfeasible to be injected in routine imaging studies in patients,[2–4,29–32] and (ii) the low signal sensitivity of the nuclear magnetic resonance techniques. For these reasons, the use of biocompatible probes combined with signal enhancement techniques offers great potential. MRS and MRI stands out as highly versatile and valuable tools for a wide array of applications including human imaging, *in vitro* and *in vivo*

[a]*NMR Signal Enhancement Group, Max Planck Institute for Multidisciplinary Sciences, Am Fassberg 11, 37077 Göttingen, Germany. E-mail: stefan.gloeggler@mpinat.mpg.de*
[b]*Center for Biostructural Imaging of Neurodegeneration, University Medical Center Göttingen, Von-Siebold-Str. 3A, 37075 Göttigen, German*

†Electronic supplementary information (ESI) available: Experimental section. See DOI: https://doi.org/10.1039/d4an00832d

chemical and biochemical studies, and unraveling molecular structures. Despite its remarkable capabilities, its effectiveness is hindered by its inherent low sensitivity.[33] However, this limitation is effectively addressed through hyperpolarized (HP) magnetic resonance. HP enhances MRS signals by over four orders of magnitude[34] relying on the generation of isotopically enriched, non-toxic contrast agents that enable *in vitro* and *in vivo* metabolic kinetics studies in real-time and that have been used among other for patient pH imaging.[34–36] To generate hyperpolarized ^{13}C metabolites, two approaches are largely employed. Between them, dissolution Dynamic Nuclear Polarization (dDNP) is a technique that has been used for producing HP pyruvate,[37,38] and also to produce HP bicarbonate to perform *in vitro* and *in vivo* pH measurements.[2,39–44] However, clinical scale dDNP is expensive and it is a slow technique that requires times between ten minutes to hours to produce HP metabolites.[45,46] Although several HP probes were successfully developed using dDNP, the needed of sophisticated and expensive equipment, as well as, the long polarization times are most likely the reasons why translation is challenging.[2,3,40–42,47–54] An alternative approach to hyperpolarize metabolites is based on parahydrogen-induced polarization (PHIP). This technique converts the nuclear spin singlet of parahydrogen (pH_2) into enhanced signals within seconds. One of the pH_2-based hyperpolarization methods, known as Signal Amplification by Reversible Exchange (SABRE), operates through reversible exchange processes between a target molecule and a metal catalyst.[55] For the classical PHIP method, an unsaturated precursor is required to which hydrogen is added. The development of PHIP-SAH (PHIP by means of the Side Arm Hydrogenation) opened up new opportunities to hyperpolarize metabolites.[46] Thereby, the target molecule is functionalized with an unsaturated side arm, *e.g. via* esterification. The molecule with the side arm serves as an efficient precursor to which the parahydrogen is added and this approach has demonstrated the highest yielding levels of polarization with pH_2 so far. In particular fully deuterated precursors have shown to deliver optimal polarization conditions due to the reduction of dipolar couplings to hydrogen originating from parahydrogen, prolonging T_1.[56] Overall, the unsaturated bond is hydrogenated by using pH_2 and a catalyst, usually in organic solvents. Next, the yielded proton spin order is transferred to a target ^{13}C nucleus. In our work we use the spin order transfer sequence called MINERVA (Maximizing Insensitive Nuclei Enhancement Reached *Via* parahydrogen Amplification) for this transfer.[56] Following the magnetization transfer, the side chain is removed by hydrolysis enabled by the addition of a base. The organic solvent is removed by evaporation and after subsequent filtration, the pH is adjusted to physiological values, and finally, after around one minute, the HP ^{13}C-compound is obtained.[34] The procedures including used precursors are shown in Fig. 1A and PHIP-SAH has overall allowed to enhance important metabolites for *in vivo* studies.[34–36,46,57–64] Thereby ^{13}C-pyruvate is used as key metabolite for a non-invasive kinetic evaluation of conversions from pyruvate to lactate in real-time *in vitro* and *in vivo*.[34,56,59,65] Even though metabolites and especially pyruvate can be hyperpolarized with parahydrogen, so far, no biocompatible parahydrogen derived pH sensor is available at sufficient polarization (>10% ^{13}C polarization). The latter we are introducing in this work by performing a non-enzymatic decarboxylation in which H_2O_2 present a nucleophilic addition to the α-carbonyl group of pyruvate to generate an unstable intermediate, which reacts to CO_2 that is in equilibrium with HCO_3^-, acetate, and water at neutral pH (Fig. 1B).[35,66]

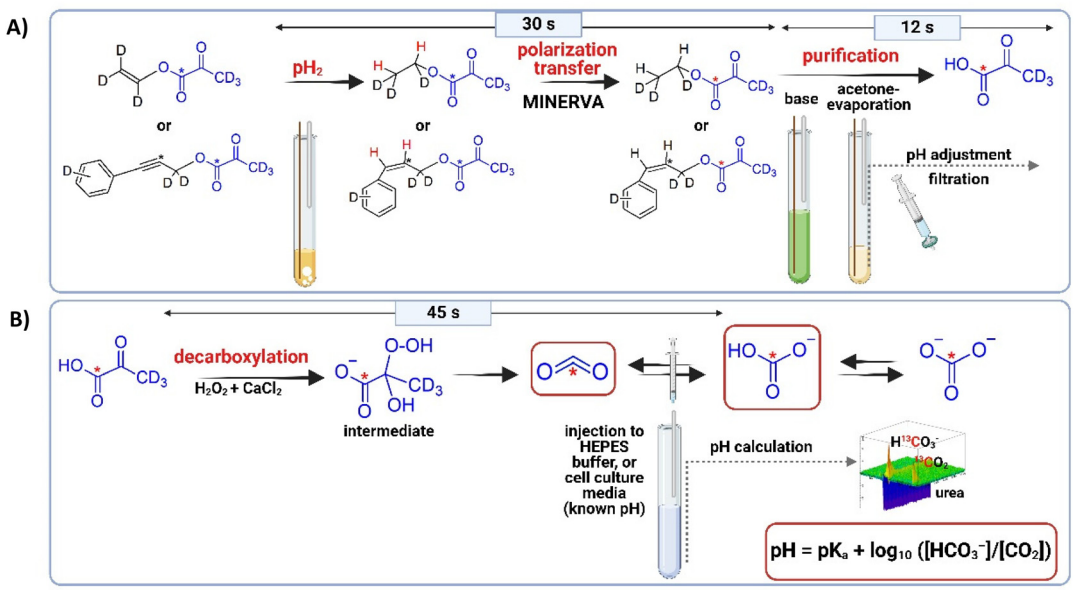

Fig. 1 Schematic representation of the PHIP-SAH workflow; (A) full workup that includes: pH_2 bubbling (20 s), MINERVA polarization transfer (10 s), base addition (1 s), acetone evaporation (8 s), buffer addition (1 s) and filtration (3 s); (B) decarboxylation process to obtain PHIP-$H^{13}CO_3^-$/PHIP-$^{13}CO_2$ (reaction takes 45 s), and pH measurement at 7 T. Own Fig. created with BioRender.com.

Materials and methods

Chemicals

All chemicals were purchased from Sigma Aldrich, except the precursors that were synthesized according to published procedure.[35,61,67] Please refer to the ESI† for further information (Schemes S1 and S2†).

Hyperpolarization and non-enzymatic decarboxylation: procedure and equipment

[1,4-Bis(diphenylphosphino)butane](1,5-cyclooctadien)rhodium(I)-tetrafluorborat (Sigma Aldrich, catalog # 79255-71-3) was dissolved in acetone-d_6 and used as catalyst for the PHIP procedure with a final concentration of 10 mM. After mixing with the precursor (vinyl pyruvate-d_6 at 50 mM or phenyl propargyl pyruvate ester-d_6 at 5.5 mM), the samples were filled into a 7-inch 5 mm NMR tube and bubbled with N_2 for 10 seconds for degassification. *para*-enriched hydrogen was obtained at 20 K with a He-cooled parahydrogen generator provided by a Cryocooler system (Sumimoto HC-4A helium compressor, Sumimoto Cold Head CH-204 with pH_2 reaction chamber by ColdEdge Technologies, temperature controller Lake Shore Cryotronics, Inc.) and delivered by a home-built valve and tubing system. Hyperpolarization and polarization transfer were carried out in a Bruker Avance III HD 300 narrow bore spectrometer operating at 7.05 T field strength equipped with a room temperature broadband observe (BBO) probe head for sample diameters of 5 mm (PA BBO 300S1 BBF-H-D-05 Z). Vinyl pyruvate-d_6 was hyperpolarized by using the MINERVA sequence as described previously (detailed in the ESI, Fig. S2A and B†).[35,65] For hyperpolarization of phenyl propargyl pyruvate ester-d_6, a field-independent MINERVA sequence for the transfer of longitudinal spin order of parahydrogen polarization was applied as previously published (detailed in the ESI†).[36] After finalization of both processes (30 s), 200 μL of a Na_2CO_3 in D_2O (75 mM for 50 mM of the vinyl pyruvate-d_6 precursor or 7.5 mM for 5.5 mM of the phenyl propargyl pyruvate ester-d_6 precursor), containing EDTA (1 mM in D_2O, which prolongs T_1 and stabilize the polarization),[68] and sodium ascorbate (50 mM in D_{2O}, which decreases the polarization loss),[69] were added to cleave the side arm and release hyperpolarized [1-^{13}C]pyruvate-d_3. Then, the NMR tube was placed outside the magnet and acetone was evaporated by passing N_2 at 7 bar pressure through the tube, and by immersing the tube in warm water (~79 °C) for 8 seconds.[34] After evaporation, indicated by a reduction of the total volume by one half in these 8 s (the volume of acetone and base added were 200 μL each, so the reduction of the acetone volume was visually checked), 50 μL of HEPES (100 mM, pH 10 in D_2O) were added to obtain physiological conditions in the final solution (1 s). The aqueous solution was then filtered from the NMR tube into a syringe by using a PVDF filter with a pore size of 1.0 μm (Fisher Scientific) to obtain in 3 s the catalyst-free signal-enhanced [1-^{13}C]pyruvate-d_3.[34] Finally, 50 μL of H_2O_2 at 326 mM (final concentration 50 mM, 0.15%) was added to induce the non-enzymatic decarboxylation. 25 μL $CaCl_2$ at a concentration of 3 mM was injected together with H_2O_2 to increase the decarboxylation rate. Fig. 1 and Fig. S1 (ESI)† show a schematic representation of the entire procedure. In Fig. 2 is shown the spectrum recorded after 45 s of the reaction.

Monitoring of pyruvate decarboxylation

The decarboxylation reaction of pyruvate was followed spectroscopically at 50 °C using a series of 90° single scan ^{1}H NMR at 7 T every 5 s, after mixing 30 mM of Sodium pyruvate in D_20 (concentration of pyruvate expected in the decarboxylation solution when starting from 50 mM in hyperpolarization experiments due to dilution by addition of buffer, H_2O_2, and $CaCl_2$), with 50 mM of H_2O_2, and 3 mM of $CaCl_2$ both in D_2O. The integral intensities of the ^{1}H signals of the methyl group of each species were converted to concentrations. Below is detailed the model described by Tickner *et al.* (2020),[70] followed for the respective equations:

$$\mathrm{B} \underset{k_{\mathrm{HY}}}{\overset{k_{-\mathrm{HY}}}{\rightleftharpoons}} \mathrm{A} \xrightarrow[+\mathrm{H_2O_2}]{k_{\mathrm{H_2O_2}}} \mathrm{C}$$

$$[\mathrm{A}]_{t+\delta t} = [\mathrm{A}]_t + (-k_{\mathrm{H_2O_2}}[\mathrm{A}]_t[\mathrm{D}]_t - k_{\mathrm{Hy}}[\mathrm{A}]_t + k_{\text{-Hy}}[\mathrm{B}]_t)\partial t$$

$$[\mathrm{B}]_{t+\delta t} = [\mathrm{B}]_t + (k_{\mathrm{Hy}}[\mathrm{A}]t - k_{\text{-Hy}}[\mathrm{B}]_t)\partial t$$

$$[\mathrm{C}]_{t+\delta t} = [\mathrm{C}]_t + (k_{\mathrm{H_2O_2}}[\mathrm{A}]_t[\mathrm{D}]_t)\partial t$$

$$[\mathrm{D}]_{t+\delta t} = [\mathrm{D}]_t - (k_{\mathrm{H_2O_2}}[\mathrm{A}]_t[\mathrm{D}]_t)\partial t$$

where A represents sodium pyruvate, B is pyruvate hydrate, C is acetate, and D is the rate of reaction between pyruvate and H_2O_2 obtained by fitting the integral intensities of ^{1}H CH_3 resonances of A, B, and C. $k_{-\mathrm{Hy}}$, k_{Hy}, and $k_{\mathrm{H_2O_2}}$ are the rates of each reaction, and in the equations δt is an incremental time difference.

As described by Tickner *et al.* (2020),[70] rate constants were found by minimizing the differences between concentrations

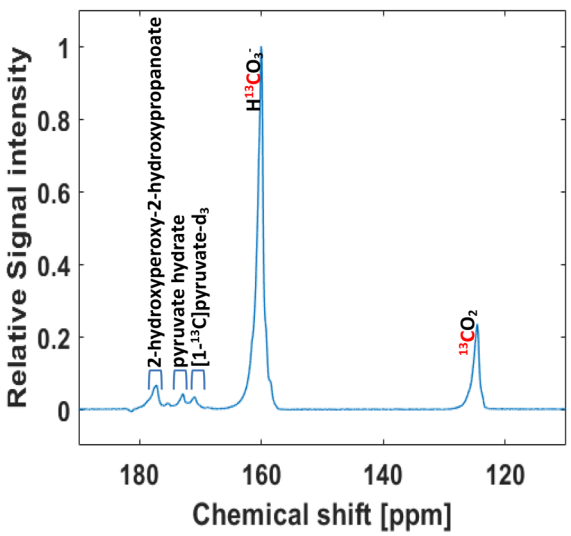

Fig. 2 Non-enzymatic decarboxylation of HP [1-^{13}C]pyruvate-d_3 (50 mM) with H_2O_2 (50 mM) at 50 °C. Single ^{13}C spectrum recorded at 7 T after 45 s of H_2O_2 injection.

determined experimentally and the calculated values. We also maintained the same assumptions, in which species as H_2O, pyruvate dimers or enol pyruvate, and the pathway that allows pyruvate hydrate reaction with H_2O_2 were not included in the model. In the ESI† are detailed the obtained kinetic parameters and the fitting (Table S1 and Fig. S3†).

PHIP $H^{13}CO_3^-/^{13}CO_2$ pH measurements in phantoms

HEPES buffer solutions in D_2O were prepared at different pH values (6.40, 6.50, 6.61, 6.70, 6.81, 6.90, 7.20, and 7.40). The pH of each solution was adjusted using HCl (100 mM in D_2O) and NaOH (100 mM in D_2O), as necessary, and verified using a calibrated pH electrode. The pH measurements were performed in a Bruker Avance IV 300 7.05 T wide bore spectrometer equipped with a MicWB40 rf probe and Micro 2.5 WB gradient system at room temperature. The phantom consisted in eight empty NMR tubes labelled from 1–8 and placed surrounding a urea phantom tube, which was used as a positioning reference (Fig. 4A). 350 μL of HEPES at pH 6.4 were injected into tube 1, immediately before the injection of 175 μL of the $H^{13}CO_3^-/^{13}CO_2$ (5.5 mM). After injection of $H^{13}CO_3^-/^{13}CO_2$, we conducted non-localized spectroscopic experiments with low-flip angle excitations to obtain the $H^{13}CO_3^-/^{13}CO_2$ integrals. Specifically, seven seconds after injection, a train of 20° flip angle pulses was initiated and a spectrum was acquired every 3 seconds. After achieving the steady state (state in which the rates of the forward and reverse reactions are equal, leading to constant concentrations of the involved species), the pH value of the respective tube was calculated by using the Henderson–Hasselbalch equation (more details in the ESI†). This procedure was repeated for each subsequent tube (2–8) to conduct the pH measurements. Each experiment was separated by a 5-minute interval to ensure that no residual signal was detected from the previous tube. This interval allowed any potential HP signal to dissipate, ensuring accurate readings. Once the pH measurements were finished for all the tubes, 500 μL of H_2O were injected into each tube to obtain a representative ^1H image of the setup (Fig. 4A). For this, a FLASH sequence (fast low angle shot magnetic resonance imaging) with a field of view of 30 × 30 mm^2, a matrix size of 256 × 256, and a central slice with 3 mm thickness in the transversal plane were used. Finally, the ^1H image and pH values obtained from the spectroscopic measurements were employed to generate a pH color-representative graph using MATLAB software (Fig. 4B).

PHIP $H^{13}CO_3^-/^{13}CO_2$ pH measurements in cell culture media

Mouse pancreatic ductal adenocarcinoma cell line (PanC02) were kindly provided by Professor Stine Pedersen (University of Copenhagen) and Professor Frauke Alves (MPI NAT, Goettingen), and they were cultured in DMEM without bicarbonate, with HEPES, supplemented with 10% Fetal bovine Serum, and 1% penicillin/streptomycin, at 37 °C, 5% CO_2 in a humidified incubator. After four days *in vitro*, cell culture media was collected from different flasks and the pH was measured with a pH-electrode. Furthermore, fresh media-pH was also measured with the electrode. Immediately after that, we carried out pH measurement with our probe, using identical conditions as detailed before for phantoms measurements. Table S4 in the ESI† shows the individual pH values obtained for each experiment.

Measurement of polarization and T_1

Polarization values were determined from six independent experiments, by comparing the signal intensity from one hyperpolarized sample recorded with a 90° pulse to a spectrum measured at thermal equilibrium. The thermal spectrum was measured with the same acquisition parameters, T = 290 K using 160 scans. Peak areas from the hyperpolarized spectra were corrected according the flip angle (20°) and fitted to a decaying exponential to approximate T_1 values.

Data analysis, % polarization calculation, and statistics

The spectra were processed using TopSpin software version 4.0.8. Phase correction, line-broadening (LB 5 for EM), and baseline corrections were applied. Further analyses and 3D plot were performed using MATLAB software version R2019b. In each spectrum, the peaks of HCO_3^- and CO_2 were integrated to determine the area under the curves (AUCs). From the ratio of the AUCs, pH values were calculated by using Henderson–Hasselbalch equation. Correlation and statistical analysis were perform in GraphPad Prism version 9 software.

Polarization level was calculated using the following equation:

$$P_{hyp} = \frac{I_{hyp}}{I_{th}} \times \frac{rg_{th}}{rg_{hyp}} \times \frac{ns_{th}}{ns_{hyp}} \times \frac{\sin(\theta_{th})}{\sin(\theta_{hyp})} \times P_{th}.$$

In this equation, P_{hyp} represents the polarization level of the sample in the hyperpolarized spectra, and P_{th} the polarization value of the sample in the thermal spectra. I represents the integration in the same spectra region (*e.g.* ^{13}C NMR signal of pyruvate at around 170 ppm) in both, hyperpolarized (I_{hyp}) and thermal spectra (I_{th}). rg is the receiver gain of the spectrometer, $\sin(\theta_{th})$ = 1 and ns_{hyp} = 1, as the thermal experiments were acquired with a flip angle of 90° degrees, and a singles scan is used in hyperpolarization experiments. A comparison between one single ^{13}C scan recorded for 50 mM of hyperpolarized (HP) [1-^{13}C]-pyruvate-d_6 and its corresponding thermal spectrum is showed in the ESI (Fig. S4).†

To calculate polarization levels for the $H^{13}CO_3^-/^{13}CO_2$ species, we took the most conservative calculation using $H^{13}CO_3^-/^{13}CO_2$ integrals after purification workup, and 45 s after H_2O_2 injection, in at least three different experiments.

Results and discussion

PHIP pH probe development

In this work, a $H^{13}CO_3^-/^{13}CO_2$ probe was developed to measure extracellular pH. This probe was obtained in D_2O at physiological conditions by non-enzymatic decarboxylation of signal enhanced 1-^{13}C-pyruvate (see Fig. 1B).[35] Fully deuterated

precursors were used to restrict the effective nuclear spin system and minimizing the loss of signal enhancement.[35] In a first step the hyperpolarization of [1-^{13}C]pyruvate-d_3 obtained from vinyl pyruvate-d_6 was optimized and an average polarization of 36.65 ± 0.06% (see ESI†) was obtained starting from 50 mM 1-^{13}C-vinyl pyruvate-d_6 precursor. It is worth to mention that the highly obtained polarization on pyruvate would enable the preparation of the metabolic probes with liquid nitrogen cooled parahydrogen for which polarization levels would be a factor of three less but still exceed 10% ^{13}C polarization. Note that this is the measured polarization of purified pyruvate in D_2O. The purification procedure was performed by cleavage of the side arm with Na_2CO_3 (75 mM) supplemented with EDTA (1 mM), and sodium ascorbate (50 mM). After obtaining free [1-^{13}C]pyruvate-d_3 at 50 °C, the pH was adjusted to biocompatible conditions with HEPES-buffered D_2O. Followed by pH adjustment, H_2O_2 was added to induce the non-enzymatic decarboxylation, together with $CaCl_2$ to increase the decarboxylation rate.[2,71,72] We also investigated our previously introduced Phenyl propargyl pyruvate ester precursor (PPE) at high field together with a field-independent pulsed PHIP-SAH method, which however yielded low degrees of pyruvate polarization. The complete process yielded 2.45 ± 0.01% pyruvate polarization that might be due to reduced relaxation times as compared to low field applications.[36]

We attribute that remarkable polarization value achieved on [1-^{13}C]pyruvate-d_3 starting from vinyl pyruvate-d_6 to some changes implemented in the purification and pH stabilization procedure. In contrast to previous purification methodologies employed by us,[34–36,56,65] that involved the use of Na_2CO_3 (100 mM) in H_2O, the present methodology employed the same base, but in D_2O, with a concentration of 75 mM, and supplemented with EDTA (which prolongs T_1 and stabilize the polarization, according to dDNP experiments),[68] and sodium ascorbate (which decreases the polarization loss during cleavage as previously reported).[69] Notably, the evaporation procedure involved the use of N_2 bubbling, differing from the conventional vacuum-assisted evaporation.[36]

The final adjustment of pH was performed through the addition of HEPES dissolved in D_2O, departing from the prior use of HEPES in H_2O. It was reported that retaining pyruvate in PBS-D_2O, instead of PBS-H_2O leads to lengthening of relaxation times which may play a crucial role in this process.[45] Moreover, in a recently published study, a similar effect was observed when $H^{13}CO_3^-/^{13}CO_2$ were obtained *via* hydrolysis of HP [1-^{13}C]1, 2-glycerol carbonate. Hydrolysis conducted with NaOH in D_2O affords superior polarization values and extended lifetimes compared to its counterpart in H_2O.[52] In this point, it is important mentioning that D_2O is safe for *in vivo* and humans injection, as was previously informed.[45,73] In a next step, we added H_2O_2 (50 mM) and found that after 45 s the reaction intermediates had sufficiently been converted into $H^{13}CO_3^-/^{13}CO_2$. A total ^{13}C polarization of 12.46 ± 0.01% was estimated based on the initial ^{13}C thermal signal of the precursor. Fig. 2 illustrates a ^{13}C spectrum recorded at 7 T using a single-90 degree pulse, post-purification, and subsequent to 45 s of H_2O_2 injection. $H^{13}CO_3^-/^{13}CO_2$ are the main species present, together with small traces of [1-^{13}C]pyruvate-d_3 (~171 ppm), the intermediate (2-hydroxyperoxy-2-hydroxypropanoate, ~176 ppm), and pyruvate hydrate (~178 ppm).[35,74]

[1-^{13}C]pyruvate-d_3 decarboxylation kinetics

Furthermore, we monitored the sodium pyruvate decarboxylation rate following the model previously reported by Tickner *et al.*[70] Briefly, 30 mM of sodium pyruvate (concentration expected in the decarboxylation solution when starting from 50 mM in hyperpolarization experiments) were decarboxylated by the addition of 50 mM of H_2O_2 in D_2O and 3 mM of $CaCl_2$ in D_2O. The reaction was monitored spectroscopically at 50 °C using a series of 90° single scan ^{1}H NMR at 7 T every 5 s. The integral intensities of pyruvate, acetate, and pyruvate hydrate were converted to concentration and plotted over time (see ESI†). By fitting these data to the kinetic model described by Tickner *et al.* using the same assumptions (*e.g.* omission of H_2O, pyruvate dimers, or enol pyruvate species, as well as, omission of the reaction between pyruvate hydrate and H_2O_2),[70] the rate of the reaction between pyruvate and H_2O_2 was calculated. The $k_{H_2O_2}$ value was estimated as (0.88 ± 0.14) $dm^3\ mol^{-1}\ s^{-1}$ (please refer to the ESI† for further details). Even though this value demonstrate a rapid decarboxylation rate of pyruvate, and pyruvate conversion was approximately of 76%. 9 mM of uncarboxylated pyruvate (24%) were present after 45 s of H_2O_2 addition. Given the signal strengths shown in Fig. 2 we do not expect interferences due to the low concentration. However, if it is considered that uncarboxylated pyruvate could be transformed *in vivo* to lactate (~182 ppm) and alanine (~176 ppm), there are no major concerns since the residual products will not interfere with the signal of the species used for the pH measurements $H^{13}CO_3^-$ (~160 ppm), and $^{13}CO_2$ (~128 ppm), and actually could provide valuable information about real-time metabolic kinetics. Concerning H_2O_2 concentration, assuming a 1 : 1 relation between acetate formed and H_2O_2 consumed, it was observed that at 45 s the remaining concentration of H_2O_2 is approximately 20 mM (0.06%) in 325 μL. Human studies exist in which H_2O_2 in concentrations between (0.06–0.48)% were injected *via* intra-arterial or intravenous (evaluating its therapeutic potential on head and neck cancer, arteriosclerosis, wound healing) did not show toxicity.[75] On *in vivo* experiments, the reported intravenous (median lethal dose) LD_{50} in mice was founded to be 50 000 mg per kg body weight.[76] Therefore, given that facts, and the fact that that our solution would dilute by the blood volume (~6 L in humans, 77–80 μL g^{-1} in mice), the residual concentration does not appear to pose a concern to humans or mice. Nevertheless, upon a potential advancement into clinical trials these procedures would need to be optimized by ideally further reducing the H_2O_2 content and performing a toxicology assessment.

Regarding $CaCl_2$ at the final solution, this is added during decarboxylation at 3 mM, concentration that is much lower than used safely in humans and mice for calcium replenishment in arrhythmias associated with hypocalcemia, hyperkale-

mia, an antidote for magnesium poisoning, as co-adjuvant in hemostatic agents preparations, as well as, to resolve refractory hypotension and complete heart block, *etc*.[77–81] Additionally, Kawai *et al.* (2011) reported the use of $CaCl_2$ injected intravenously (*via* tail vein) in mice to show how this compound accelerate wound healing. In these experiments a dose of 0.6 mg per mouse was used without any observed side effects.[82] In our injections, even if all the initial $CaCl_2$ were present in the final solution, it will represent a dose of 0.0033 mg per mouse, so side effects are unlikely. Respect to rhodium residuals, we have previously reported that the levels at the final solution after filtration is (17 ± 5) μM.[56] This concentration have not generated any side effects *in vivo* or toxicity in cells experiments, even when double injection of the probe was used.[34,56,59,65] Finally, acetate is expected to be present in the final solution. However, it has been previously reported the use of hyperpolarized acetate as a tracer in different diseases and events (*e.g.* diabetes, cardiac and renal metabolism, glioma, *etc*.) on *in vivo* and human studies demonstrating that this compound does not pose challenges.[83–87] In addition to that, acetate-buffers were extensively used as first-line intravenous resuscitation fluids in patients, for example during hemorrhagic shock.[88–90]

PHIP $H^{13}CO_3^-/^{13}CO_2$ validation in phantoms

During *in vivo* experiments, [1-^{13}C]pyruvate-d_3 is injected into the mouse's tail vein, thus suffering a dilution because of the mouse blood volume. Considering that the approximate blood volume of a mouse is 77–80 μL g^{-1},[91,92] and that in our previous *in vivo* experiments with pyruvate usually C57BL6 mice with a weight of ~20 g (10–12 weeks) are used,[34,65] the final concentration of biomarkers when injected into the vein tail (volume injected ~50–100 μL) will decrease about by a factor of ten.

Taking that into account, we wanted to evaluate the accuracy of the pH sensor at a 10-fold lower concentration. Following establishment of the procedure, pH measurements of eight phantoms were performed in a 7 T imaging spectrometer (more details in the ESI†). Each phantom contained HEPES buffers at different pH (6.40, 6.50, 6.61, 6.70, 6.81, 6.90, 7.20, and 7.40) in D_2O. After filtration and decarboxylation, the solution containing $H^{13}CO_3^-/^{13}CO_2$ was injected into the different tubes (one by one, and after an interval of 5 min, as explained in Materials and Methods section) containing the mentioned buffers. Upon injection, ^{13}C-spectra were acquired with low-flip angle excitations (20°) to obtain $H^{13}CO_3^-/^{13}CO_2$ integrals (Fig. 3 shows one example). Once achieving the steady state (state with constant concentration, according to two-way ANOVA followed by the Bonferroni's test for multiple comparisons), pH was calculated by using the Henderson–Hasselbalch equation: $pH = 6.2 + \log([HCO_3^-]/[CO_2])$,[93] and the ratio of the $H^{13}CO_3^-/^{13}CO_2$ integrals. Table 1 shows the means ± SD for $H^{13}CO_3^-/^{13}CO_2$-measured pH values and their corresponding electrode-measured values, obtained after three independent experiments. Following spectroscopic measurements, the pH of the final solutions was determined

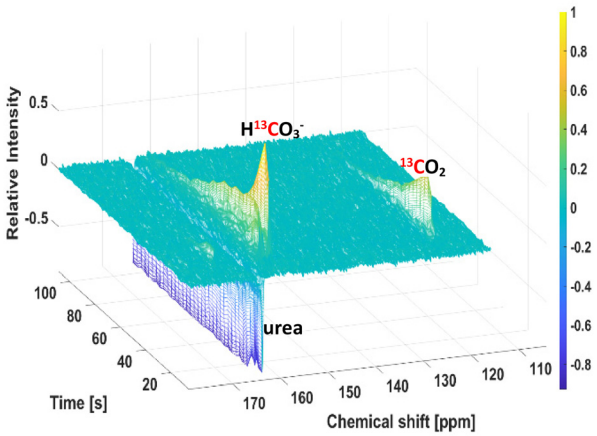

Fig. 3 Example for a time series of ^{13}C NMR spectra recorded with a flip angle of 20° upon injection of signal-enhanced $H^{13}CO_3^-/^{13}CO_2$ in a phantom of pH 6.5, after non-enzymatic decarboxylation of hyperpolarized [1-^{13}C]pyruvate-d_3. A urea phantom was used in order to ensure correct position of the phantom tubes during the measurements, and its signal is in antiphase showing non-hyperpolarization.

Table 1 Measured pH by using our probe and spectroscopic data, and pH measured with an electrode

Phantom #	Electrode pH (Mean ± SD)	PHIP $H^{13}CO_3^-/^{13}CO_2$ pH (Mean ± SD)
1	6.40 ± 0.01	6.37 ± 0.01
2	6.50 ± 0.01	6.50 ± 0.05
3	6.61 ± 0.01	6.60 ± 0.007
4	6.70 ± 0.01	6.65 ± 0.02
5	6.81 ± 0.01	6.76 ± 0.03
6	6.90 ± 0.01	6.91 ± 0.06
7	7.20 ± 0.01	7.15 ± 0.01
8	7.40 ± 0.01	7.35 ± 0.07

with a pH electrode, and the values were in good agreement with those determined from the spectroscopic data (Table 1). This pH sensor methodology demonstrates accuracy with standard deviations lower than 0.07 pH units (expanded details in the ESI†).

Likewise, $H^{13}CO_3^-/^{13}CO_2$ pH values did not differ significantly from the electrode-measured ones, according to two-way ANOVA followed by the Bonferroni's test for multiple comparisons. Fig. 4A shows a ^{1}H image of our measurement setup (as explained in Materials and Methods). To ensure the correct position of the tubes, a urea-^{13}C phantom was placed in the center. In (B) a color map represents the pH values obtained with our probe. (C) and (D) shows the correlation between the mean of $H^{13}CO_3^-/^{13}CO_2$ pH values obtained from three independent experiments and electrode pH. The close correlation obtained reflects a rapid establishment of chemical equilibrium and equilibration of polarization between the $H^{13}CO_3^-/^{13}CO_2$ species. Although previous studies reported a difference of ~0.3 pH units where the $H^{13}CO_3^-/^{13}CO_2$ pH was higher than the electrode-measured pH in the absence of the

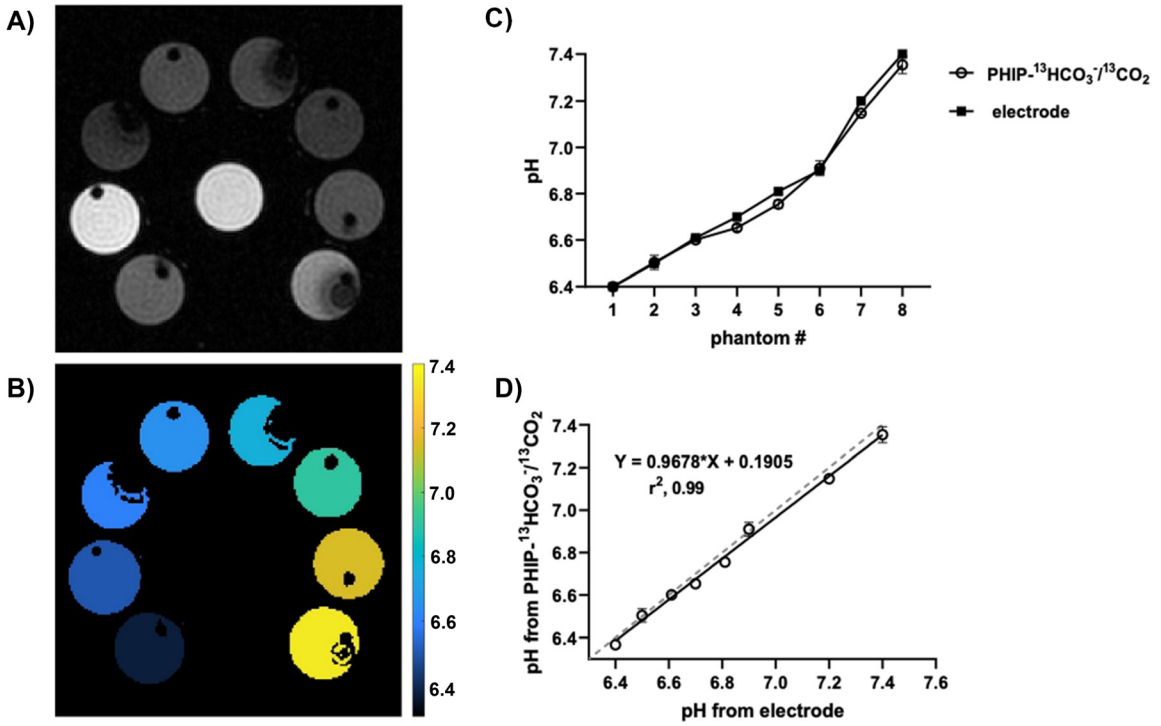

Fig. 4 (A) Proton imaging of the setup acquired at the end of the measurements by adding H_2O to all the measured tubes. The tube in the center corresponds to a urea phantom, which was used as a positioning reference. (B) Color graphical representation of the pH values generated in MATLAB software by using the pH values obtained spectroscopically from the ratio of hyperpolarized $H^{13}CO_3^-/^{13}CO_2$ integrals, and the ^1H image showed in A. (C) pH *vs.* phantom number (#) for PHIP $H^{13}CO_3^-/^{13}CO_2$-pH and electrode-pH. No statistically differences were found after analysis by two way ANOVA followed by the Bonferroni's test for multiple comparisons using GraphPad Prism 9 software. (D) Correlation of the PHIP $H^{13}CO_3^-/^{13}CO_2$-pH from spectroscopic data with the values measured using a pH electrode. A solid linear regression line with its corresponding equation is shown for the measured pH with our probe, and a dashed line that represents direct proportionality between the two variables.

enzyme carbonic anhydrase (by using voxel by voxel estimation),[39] we did not observe the same effect in our spectroscopic data. Our hypothesis relies on an improvement of T_1,[45,52] attributable to the generation of the signal-enhanced $H^{13}CO_3^-/^{13}CO_2$ in D_2O (instead of H_2O).

The T_1 values for these species in D_2O at 7 T and room temperature were (54.3 ± 9.7) s for $H^{13}CO_3^-$, and (49.0 ± 3.0) s for $^{13}CO_2$. This might facilitate a rapid exchange between $H^{13}CO_3^-/^{13}CO_2$, and the rate of polarization loss for both species becomes similar (according to *t*-student, *p*-value from the comparison of the T_1 values is 0.2, not statistically different). That rapid interconversion could contribute to maintain pH values during the steady state as is shown in Fig. 5, increasing the accuracy of the measurements.[2] Another fact that could contribute to the improved correlation between PHIP $H^{13}CO_3^-/^{13}CO_2$-pH and electrode-pH, is based on the use of an alkaline buffer (pH = 10) in our procedure to achieve physiological conditions (pH = 7), this step would be responsible for reducing CO_2 losses prior to injection.[3]

PHIP $H^{13}CO_3^-/^{13}CO_2$ validation in cell culture media

In order to test our probe in a more biological-complex environment, pH measurements were conducted in conditioned media from pancreatic cancer cells (PanC02 cell line)

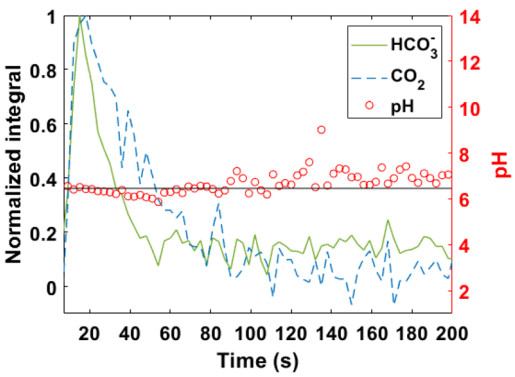

Fig. 5 Profile of normalized integral (arbitrary unit) of $H^{13}CO_3^-$ and $^{13}CO_2$, and pH *vs.* time, after injection of signal-enhanced $H^{13}CO_3^-/^{13}CO_2$ into a HEPES phantom of pH 6.5. pH values from the steady state were selected to calculate the ones showed in Table 1.

corresponding to 4 days *in vitro* (div). These measurements were compared with fresh media containing all the same supplements than the media used for PanC02 culture. Specifically, the media used was DMEM high glucose, without bicarbonate supplemented with 10% fetal bovine serum and 1% penicillin/streptomycin. Fig. 6 shows the correlation of the PHIP

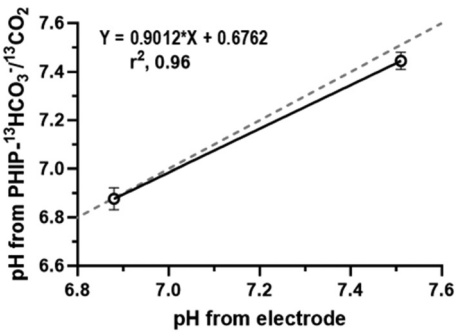

Fig. 6 Correlation PHIP $H^{13}CO_3^-/^{13}CO_2$-pH and electrode-pH values obtained from cell culture media. A solid linear regression line and equation is shown for the measured $H^{13}CO_3^-/^{13}CO_2$-pH, the dashed line that represents direct proportionality between the two variables.

$H^{13}CO_3^-/^{13}CO_2$-pH from spectroscopic data with the values measured using an electrode.

The mean for pH values measured with our probe are summarized in Table 2 (please see the ESI† for more details).

In this case, accurate pH values were also found in agreement with those measured by using the electrode.

Lastly, we present a probe prepared by using highly polarized pyruvate (36.65%), and a non-enzymatic decarboxylation reaction to achieve the $H^{13}CO_3^-/^{13}CO_2$ pH sensor, with a polarization value of 12.46%. It is important to note that the polarization losses for the $H^{13}CO_3^-/^{13}CO_2$ sensor can be attributed mainly to relaxation effects (T_1 54.3 s for $H^{13}CO_3^-$, and 49.0 s for $^{13}CO_2$), which could be further improved in the future by optimized reactions in an automatized setup. We have validated our probe *in vitro* by measuring pH on phantoms and pancreatic cancer cell media with highly accuracy. Previous $H^{13}CO_3^-/CO_2$ studies were conducted with dDNP achieving similar levels of polarization: Ghosh *et al.* (2014), reached $H^{13}CO_3^-$ with notable polarization (~16%) by employing α-keto carboxylic acid-derivatives decarboxylation with H_2O_2 and validated the probe on perfused rat lungs.[2] Besides, Mu *et al.* (2023) applied chemical reactions as hydrolysis followed by neutralization on 1,2-glycerol carbonate (GLC) to obtain $H^{13}CO_3^-$ with a polarization of ~20%, and its validation was carried out in several *in vivo* healthy and cancer mouse models.[52] Other probes derived from synthetic compounds and amino acids were developed as HP chemical-shift based pH sensors.[47,48,51,94] As mentioned above, dDNP is facing challenges on the development to routine clinical use. With respect to pH sensors for example, polarization times of 2 h are needed (probe obtained by direct polarization on $CsH^{13}CO_3$),[39] 1.5 h (probe obtained by decarboxylation of HP α-keto carboxylic acid-derivatives),[2] and 7 h (probe obtained by base-catalyzed hydrolysis followed by neutralization on ^{13}C-GLC),[52] together with all the time needed for reaction and post dilution steps. Therefore, parahydrogen based methods pose a scalable solution, as hyperpolarized agents can be rapidly produced on-site and even in portable devices. Finally, assessment of parahydrogen enhanced contrast agents in large volumes (40 mL as in dDNP) and patient studies are currently not feasible and are part of our ongoing work.

Table 2 Measured pH values in conditioned media from PanC02 cells and fresh media using our probe and spectroscopic data, and pH measured with electrodes

Media	PHIP $H^{13}CO_3^-/^{13}CO_2$ pH	Electrode pH
PanC02, 4 div	6.87 ± 0.08	6.88 ± 0.01
Fresh media	7.45 ± 0.06	7.51 ± 0.01

Conclusions

In conclusion, we present an optimized methodology to obtain biocompatible hyperpolarized $H^{13}CO_3^-/^{13}CO_2$ pH sensor within a minute using PHIP to perform pH measurements at physiological conditions with high accuracy. To achieve the probe, purified [1-^{13}C]pyruvate-d_3 with a notable ^{13}C polarization of 36.65 ± 0.06% in aqueous solution and at physiological pH is decarboxylated. For this, H_2O_2 with an addition of $CaCl_2$ yield signal-enhanced $H^{13}CO_3^-$ and $^{13}CO_2$ in D_2O with an average ^{13}C-polarization of 12.46 ± 0.01%. We attribute these remarkable polarization values to optimizations performed in our purification and pH adjustment procedures. We envision that the presented procedures, which offer advantages in polarization efficiency, accuracy, and speed, can be rapidly adopted for preclinical investigations and future clinical parahydrogen procedures for patient imaging.

Author contributions

Author contributions are the following: M. D. Santi, conceptualization, data curation, formal analysis, investigation, methodology, visualization, and writing-original draft; T. L. K. Hune, investigation, formal analysis, and writing-review and editing; G. G. Rodriguez, investigation, formal analysis, and writing-review and editing; L. M. Fries, investigation, formal analysis, and writing-review and editing; R. Mei, investigation, formal analysis, and writing-review and editing; S. Sternkopf, visualization, and writing-review and editing; Josef Elaßer investigation; and S. Glöggler, conceptualization, validation, funding acquisition, resources, supervision, and writing-review and editing. All authors have given approval to the final version of the manuscript.

Data availability

The data supporting this article have been included as part of the ESI.†

Conflicts of interest

Stefan Glöggler is co-founder of MagniKeen

Acknowledgements

The authors thank Dr Stevanato for his support with the experimental set up, and Dr Belov and the Chemical synthesis facility team for their support in the scale up of the deuterated pyruvate precursor. Pancreatic cancer cell line (PanC02) kindly provided by Professor Stine Pedersen from University of Copenhagen. This project has received funding from the European Research Council (ERC) under the European Union's Horizon 2020 research and innovation program (Grant Agreement No. 949180). Stefan Glöggler acknowledges funding by the Max Planck Society and the German Research Foundation (DFG) under Grant 495627437, 491827624 and 450146057.

References

1 E. Hopkins, T. Sanvictores and S. Sharma, *StatPearls*, Treasure Island (FL), 2024.
2 R. K. Ghosh, S. J. Kadlecek, M. Pourfathi and R. R. Rizi, Efficient production of hyperpolarized bicarbonate by chemical reaction on a DNP precursor to measure pH, *Magn. Reson. Med.*, 2015, **74**, 1406–1413.
3 F. A. Gallagher, M. I. Kettunen and K. M. Brindle, Imaging pH with hyperpolarized 13C, *NMR Biomed.*, 2011, **24**, 1006–1015.
4 R. J. Gillies, N. Raghunand, M. L. Garcia-Martin and R. A. Gatenby, pH imaging. A review of pH measurement methods and applications in cancers, *IEEE Eng. Med. Biol. Mag.*, 2004, **23**, 57–64.
5 D. Czaplinska, R. Ialchina, H. B. Andersen, J. Yao, A. Stigliani, J. Dannesboe, M. Flinck, X. Chen, J. Mitrega, S. P. Gnosa, O. Dmytriyeva, F. Alves, J. Napp, A. Sandelin and S. F. Pedersen, Crosstalk between tumor acidosis, p53 and extracellular matrix regulates pancreatic cancer aggressiveness, *Int. J. Cancer*, 2023, **152**, 1210–1225.
6 F. Visioli, Y. Wang, G. N. Alam, Y. Ning, P. V. Rados, J. E. Nor and P. J. Polverini, Glucose-regulated protein 78 (Grp78) confers chemoresistance to tumor endothelial cells under acidic stress, *PLoS One*, 2014, **9**, e101053.
7 M. Kato, K. Maeda, R. Nakahara, H. Hirose, A. Kondo, S. Aki, M. Sugaya, S. Hibino, M. Nishida, M. Hasegawa, H. Morita, R. Ando, R. Tsuchida, M. Yoshida, T. Kodama, H. Yanai, T. Shimamura and T. Osawa, Acidic extracellular pH drives accumulation of N1-acetylspermidine and recruitment of protumor neutrophils, *PNAS Nexus*, 2023, **2**, pgad306.
8 O. Warburg, On the origin of cancer cells, *Science*, 1956, **123**, 309–314.
9 H. Prasad and R. Rao, Amyloid clearance defect in ApoE4 astrocytes is reversed by epigenetic correction of endosomal pH, *Proc. Natl. Acad. Sci. U. S. A.*, 2018, **115**, E6640–E6649.
10 S. W. Kuo, M. Jiang and C. Heckman, Potential involvement of intracellular pH in a mouse model of amyotrophic lateral sclerosis, *Amyotrophic Lateral Scler. Frontotemporal Degener.*, 2014, **15**, 151–153.
11 A. Rahman, B. Janic, T. Rahman, H. Singh, H. Ali, R. Rattan, M. Kazi and M. M. Ali, Immunotherapy Enhancement by Targeting Extracellular Tumor pH in Triple-Negative Breast Cancer Mouse Model, *Cancers*, 2023, **15**, 4931.
12 G. V. Martinez, X. Zhang, M. L. Garcia-Martin, D. L. Morse, M. Woods, A. D. Sherry and R. J. Gillies, Imaging the extracellular pH of tumors by MRI after injection of a single cocktail of T1 and T2 contrast agents, *NMR Biomed.*, 2011, **24**, 1380–1391.
13 R. J. Gillies, Z. Liu and Z. Bhujwalla, 31P-MRS measurements of extracellular pH of tumors using 3-aminopropylphosphonate, *Am. J. Physiol.*, 1994, **267**, C195–C203.
14 S. Gil, P. Zaderenzo, F. Cruz, S. Cerdan and P. Ballesteros, Imidazol-1-ylalkanoic acids as extrinsic ^{1}H NMR probes for the determination of intracellular pH, extracellular pH and cell volume, *Bioorg. Med. Chem.*, 1994, **2**, 305–314.
15 R. van Sluis, Z. M. Bhujwalla, N. Raghunand, P. Ballesteros, J. Alvarez, S. Cerdan, J. P. Galons and R. J. Gillies, In vivo imaging of extracellular pH using 1H MRSI, *Magn. Reson. Med.*, 1999, **41**, 743–750.
16 Z. M. Bhujwalla, D. Artemov, P. Ballesteros, S. Cerdan, R. J. Gillies and M. Solaiyappan, Combined vascular and extracellular pH imaging of solid tumors, *NMR Biomed.*, 2002, **15**, 114–119.
17 M. L. Garcia-Martin, G. Herigault, C. Remy, R. Farion, P. Ballesteros, J. A. Coles, S. Cerdan and A. Ziegler, Mapping extracellular pH in rat brain gliomas in vivo by 1H magnetic resonance spectroscopic imaging: comparison with maps of metabolites, *Cancer Res.*, 2001, **61**, 6524–6531.
18 A. K. Jindal, M. E. Merritt, E. H. Suh, C. R. Malloy, A. D. Sherry and Z. Kovacs, Hyperpolarized 89Y complexes as pH sensitive NMR probes, *J. Am. Chem. Soc.*, 2010, **132**, 1784–1785.
19 S. Aime, A. Barge, D. Delli Castelli, F. Fedeli, A. Mortillaro, F. U. Nielsen and E. Terreno, Paramagnetic lanthanide(III) complexes as pH-sensitive chemical exchange saturation transfer (CEST) contrast agents for MRI applications, *Magn. Reson. Med.*, 2002, **47**, 639–648.
20 N. Raghunand, S. Zhang, A. D. Sherry and R. J. Gillies, In vivo magnetic resonance imaging of tissue pH using a novel pH-sensitive contrast agent, GdDOTA-4AmP, *Acad. Radiol.*, 2002, **9**(Suppl 2), S481–S483.
21 D. A. Rottenberg, J. Z. Ginos, K. J. Kearfott, L. Junck, V. Dhawan and J. O. Jarden, In vivo measurement of brain tumor pH using [11C]DMO and positron emission tomography, *Ann. Neurol.*, 1985, **17**, 70–79.
22 X. Zhang, Y. Lin and R. J. Gillies, Tumor pH and its measurement, *J. Nucl. Med.*, 2010, **51**, 1167–1170.
23 V. D. Mehta, P. V. Kulkarni, R. P. Mason, A. Constantinescu, S. Aravind, N. Goomer and P. P. Antich, 6-Fluoropyridoxol: a novel probe of cellular pH using ^{19}F NMR spectroscopy, *FEBS Lett.*, 1994, **349**, 234–238.

24 R. P. Mason, Transmembrane pH gradients in vivo: measurements using fluorinated vitamin B6 derivatives, *Curr. Med. Chem.*, 1999, **6**, 481–499.
25 S. Hunjan, R. P. Mason, V. D. Mehta, P. V. Kulkarni, S. Aravind, V. Arora and P. P. Antich, Simultaneous intracellular and extracellular pH measurement in the heart by ^{19}F NMR of 6-fluoropyridoxol, *Magn. Reson. Med.*, 1998, **39**, 551–556.
26 O. Maxouri, Z. Bodalal, M. Daal, S. Rostami, I. Rodriguez, L. Akkari, M. Srinivas, R. Bernards and R. Beets-Tan, How to 19F MRI: applications, technique, and getting started, *BJR Open*, 2023, **5**, 20230019.
27 G. E. Soto, Z. Zhu, J. L. Evelhoch and J. J. Ackerman, Tumor 31P NMR pH measurements in vivo: a comparison of inorganic phosphate and intracellular 2-deoxyglucose-6-phosphate as pHnmr indicators in murine radiation-induced fibrosarcoma-1, *Magn. Reson. Med.*, 1996, **36**, 698–704.
28 D. A. Beauregard, D. Parker and K. M. Brindle, Relaxation-Based mapping of tumour pH, *International Society for Magnetic Resonance in Medicine Conference Abstract*, 1998.
29 C. F. Chang and C. C. Lin, Current concepts of contrast-induced nephropathy: a brief review, *J. Chin. Med. Assoc.*, 2013, **76**, 673–681.
30 E. Kanal and M. F. Tweedle, Residual or retained gadolinium: practical implications for radiologists and our patients, *Radiology*, 2015, **275**, 630–634.
31 T. Grobner, Gadolinium–a specific trigger for the development of nephrogenic fibrosing dermopathy and nephrogenic systemic fibrosis?, *Nephrol., Dial., Transplant.*, 2006, **21**, 1104–1108.
32 E. P. Rahrmann, D. Shorthouse, A. Jassim, L. P. Hu, M. Ortiz, B. Mahler-Araujo, P. Vogel, M. Paez-Ribes, A. Fatemi, G. J. Hannon, R. Iyer, J. A. Blundon, F. C. Lourenco, J. Kay, R. M. Nazarian, B. A. Hall, S. S. Zakharenko, D. J. Winton, L. Zhu and R. J. Gilbertson, The NALCN channel regulates metastasis and nonmalignant cell dissemination, *Nat. Genet.*, 2022, **54**, 1827–1838.
33 J. B. Hovener, A. N. Pravdivtsev, B. Kidd, C. R. Bowers, S. Gloggler, K. V. Kovtunov, M. Plaumann, R. Katz-Brull, K. Buckenmaier, A. Jerschow, F. Reineri, T. Theis, R. V. Shchepin, S. Wagner, P. Bhattacharya, N. M. Zacharias and E. Y. Chekmenev, Parahydrogen-Based Hyperpolarization for Biomedicine, *Angew. Chem., Int. Ed.*, 2018, **57**, 11140–11162.
34 T. Hune, S. Mamone, A. B. Schmidt, I. Mahú, N. D'Apolito, D. Wiedermann, J. Brüning and S. Glöggler, Hyperpolarized Multi-organ Spectroscopy of Liver and Brain Using 1-13C-Pyruvate Enhanced via Parahydrogen, *Appl. Magn. Reson.*, 2023, **54**, 1283–1295.
35 G. Stevanato, Y. Ding, S. Mamone, A. P. Jagtap, S. Korchak and S. Gloggler, Real-Time Pyruvate Chemical Conversion Monitoring Enabled by PHIP, *J. Am. Chem. Soc.*, 2023, **145**, 5864–5871.
36 S. Mamone, A. P. Jagtap, S. Korchak, Y. Ding, S. Sternkopf and S. Gloggler, A Field-Independent Method for the Rapid Generation of Hyperpolarized [1-(13) C]Pyruvate in Clean Water Solutions for Biomedical Applications, *Angew. Chem., Int. Ed.*, 2022, **61**, e202206298.
37 J. H. Ardenkjaer-Larsen, S. Bowen, J. R. Petersen, O. Rybalko, M. S. Vinding, M. Ullisch and N. C. Nielsen, Cryogen-free dissolution dynamic nuclear polarization polarizer operating at 3.35 T, 6.70 T, and 10.1 T, *Magn. Reson. Med.*, 2019, **81**, 2184–2194.
38 J. H. Ardenkjaer-Larsen, B. Fridlund, A. Gram, G. Hansson, L. Hansson, M. H. Lerche, R. Servin, M. Thaning and K. Golman, Increase in signal-to-noise ratio of > 10,000 times in liquid-state NMR, *Proc. Natl. Acad. Sci. U. S. A.*, 2003, **100**, 10158–10163.
39 F. A. Gallagher, M. I. Kettunen, S. E. Day, D. E. Hu, J. H. Ardenkjaer-Larsen, R. Zandt, P. R. Jensen, M. Karlsson, K. Golman, M. H. Lerche and K. M. Brindle, Magnetic resonance imaging of pH in vivo using hyperpolarized 13C-labelled bicarbonate, *Nature*, 2008, **453**, 940–943.
40 N. Drachman, S. Kadlecek, M. Pourfathi, Y. Xin, H. Profka and R. Rizi, In vivo pH mapping of injured lungs using hyperpolarized [1-(13) C]pyruvate, *Magn. Reson. Med.*, 2017, **78**, 1121–1130.
41 D. E. Korenchan, R. R. Flavell, C. Baligand, R. Sriram, K. Neumann, S. Sukumar, H. VanBrocklin, D. B. Vigneron, D. M. Wilson and J. Kurhanewicz, Dynamic nuclear polarization of biocompatible (13)C-enriched carbonates for in vivo pH imaging, *Chem. Commun.*, 2016, **52**, 3030–3033.
42 D. E. Korenchan, R. Bok, R. Sriram, K. Liu, R. D. Santos, H. Qin, I. Lobach, N. Korn, D. M. Wilson, J. Kurhanewicz and R. R. Flavell, Hyperpolarized in vivo pH imaging reveals grade-dependent acidification in prostate cancer, *Oncotarget*, 2019, **10**, 6096–6110.
43 N. Bogh, E. S. S. Hansen, C. O. Mariager, L. B. Bertelsen, S. Ringgaard and C. Laustsen, Cardiac pH-Imaging With Hyperpolarized MRI, *Front. Cardiovasc. Med.*, 2020, **7**, 603674.
44 M. A. M. Alixander S Khan, J. D. Kaggie, I. Horvat-Menih, T. Matys, R. F. Schulte, M. J. Locke, A. Grimmer, P. Wodtke, E. Latimer, A. Frary, M. J. Graves and F. A. Gallagher, Measuring extracellular human brain pH and amino acid metabolism with hyperpolarized [1-^{13}C]pyruvate, 2023,DOI: **10.1101/2023.03.23.23287579**.
45 H. de Maissin, P. R. Gross, O. Mohiuddin, M. Weigt, L. Nagel, M. Herzog, Z. Wang, R. Willing, W. Reichardt, M. Pichotka, L. Hess, T. Reinheckel, H. J. Jessen, R. Zeiser, M. Bock, D. von Elverfeldt, M. Zaitsev, S. Korchak, S. Gloggler, J. B. Hovener, E. Y. Chekmenev, F. Schilling, S. Knecht and A. B. Schmidt, In Vivo Metabolic Imaging of [1-(13) C]Pyruvate-d(3) Hyperpolarized By Reversible Exchange With Parahydrogen, *Angew. Chem., Int. Ed.*, 2023, **62**, e202306654.
46 F. Reineri, T. Boi and S. Aime, ParaHydrogen Induced Polarization of 13C carboxylate resonance in acetate and pyruvate, *Nat. Commun.*, 2015, **6**, 5858.
47 S. Duwel, C. Hundshammer, M. Gersch, B. Feuerecker, K. Steiger, A. Buck, A. Walch, A. Haase, S. J. Glaser, M. Schwaiger and F. Schilling, Imaging of pH in vivo using

hyperpolarized (13)C-labelled zymonic acid, *Nat. Commun.*, 2017, **8**, 15126.

48 C. Hundshammer, S. Duwel, S. S. Kocher, M. Gersch, B. Feuerecker, C. Scheurer, A. Haase, S. J. Glaser, M. Schwaiger and F. Schilling, Deuteration of Hyperpolarized (13) C-Labeled Zymonic Acid Enables Sensitivity-Enhanced Dynamic MRI of pH, *ChemPhysChem*, 2017, **18**, 2422–2425.

49 D. E. Korenchan, C. Taglang, C. von Morze, J. E. Blecha, J. W. Gordon, R. Sriram, P. E. Z. Larson, D. B. Vigneron, H. F. VanBrocklin, J. Kurhanewicz, D. M. Wilson and R. R. Flavell, Dicarboxylic acids as pH sensors for hyperpolarized (13)C magnetic resonance spectroscopic imaging, *Analyst*, 2017, **142**, 1429–1433.

50 T. Nishihara, Y. Kameyama, H. Nonaka, Y. Takakusagi, F. Hyodo, K. Ichikawa and S. Sando, A Strategy to Design Hyperpolarized (13) C Magnetic Resonance Probes Using [1-(13) C]alpha-Amino Acid as a Scaffold Structure, *Chem.–Asian J.*, 2017, **12**, 949–953.

51 C. Hundshammer, S. Duwel, D. Ruseckas, G. Topping, P. Dzien, C. Muller, B. Feuerecker, J. B. Hovener, A. Haase, M. Schwaiger, S. J. Glaser and F. Schilling, Hyperpolarized Amino Acid Derivatives as Multivalent Magnetic Resonance pH Sensor Molecules, *Sensors*, 2018, **18**, 600.

52 C. Mu, X. Liu, Y. Kim, A. Riselli, D. E. Korenchan, R. A. Bok, R. Delos Santos, R. Sriram, H. Qin, H. Nguyen, J. W. Gordon, J. Slater, P. E. Z. Larson, D. B. Vigneron, J. Kurhanewicz, D. M. Wilson and R. R. Flavell, Clinically Translatable Hyperpolarized (13)C Bicarbonate pH Imaging Method for Use in Prostate Cancer, *ACS Sens.*, 2023, **8**, 4042–4054.

53 M. Grashei, C. Hundshammer, F. H. A. van Heijster, G. J. Topping and F. Schilling, pH Dependence of T(2) for Hyperpolarizable (13)C-Labelled Small Molecules Enables Spatially Resolved pH Measurement by Magnetic Resonance Imaging, *Pharmaceuticals*, 2021, **14**, 327.

54 W. Jiang, L. Lumata, W. Chen, S. Zhang, Z. Kovacs, A. D. Sherry and C. Khemtong, Hyperpolarized 15N-pyridine derivatives as pH-sensitive MRI agents, *Sci. Rep.*, 2015, **5**, 9104.

55 D. A. Barskiy, K. V. Kovtunov, I. V. Koptyug, P. He, K. A. Groome, Q. A. Best, F. Shi, B. M. Goodson, R. V. Shchepin, A. M. Coffey, K. W. Waddell and E. Y. Chekmenev, The feasibility of formation and kinetics of NMR signal amplification by reversible exchange (SABRE) at high magnetic field (9.4 T), *J. Am. Chem. Soc.*, 2014, **136**, 3322–3325.

56 Y. Ding, S. Korchak, S. Mamone, A. P. Jagtap, G. Stevanato, S. Sternkopf, D. Moll, H. Schroeder, S. Becker, A. Fischer, E. Gerhardt, T. F. Outeiro, F. Opazo, C. Griesinger and S. Glöggler, Rapidly Signal–enhanced Metabolites for Atomic Scale Monitoring of Living Cells with Magnetic Resonance, *Chem.: Methods*, 2022, **2**, e202200023.

57 E. Cavallari, C. Carrera, S. Aime and F. Reineri, Studies to enhance the hyperpolarization level in PHIP-SAH-produced C13-pyruvate, *J. Magn. Reson.*, 2018, **289**, 12–17.

58 S. Korchak, S. Mamone and S. Gloggler, Over 50% (1)H and (13)C Polarization for Generating Hyperpolarized Metabolites-A para-Hydrogen Approach, *ChemistryOpen*, 2018, **7**, 672–676.

59 Y. Ding, G. Stevanato, F. von Bonin, D. Kube and S. Gloggler, Real-time cell metabolism assessed repeatedly on the same cells via para-hydrogen induced polarization, *Chem. Sci.*, 2023, **14**, 7642–7647.

60 S. Knecht, J. W. Blanchard, D. Barskiy, E. Cavallari, L. Dagys, E. Van Dyke, M. Tsukanov, B. Bliemel, K. Munnemann, S. Aime, F. Reineri, M. H. Levitt, G. Buntkowsky, A. Pines, P. Blumler, D. Budker and J. Eills, Rapid hyperpolarization and purification of the metabolite fumarate in aqueous solution, *Proc. Natl. Acad. Sci. U. S. A.*, 2021, **118**, e2025383118.

61 S. Korchak, S. Yang, S. Mamone and S. Gloggler, Pulsed Magnetic Resonance to Signal-Enhance Metabolites within Seconds by utilizing para-Hydrogen, *ChemistryOpen*, 2018, **7**, 344–348.

62 S. Korchak, M. Emondts, S. Mamone, B. Blumich and S. Gloggler, Production of highly concentrated and hyperpolarized metabolites within seconds in high and low magnetic fields, *Phys. Chem. Chem. Phys.*, 2019, **21**, 22849–22856.

63 L. Dagys, A. P. Jagtap, S. Korchak, S. Mamone, P. Saul, M. H. Levitt and S. Gloggler, Nuclear hyperpolarization of (1-(13)C)-pyruvate in aqueous solution by proton-relayed side-arm hydrogenation, *Analyst*, 2021, **146**, 1772–1778.

64 L. Kaltschnee, A. P. Jagtap, J. McCormick, S. Wagner, L. S. Bouchard, M. Utz, C. Griesinger and S. Gloggler, Hyperpolarization of Amino Acids in Water Utilizing Parahydrogen on a Rhodium Nanocatalyst, *Chemistry*, 2019, **25**, 11031–11035.

65 T. Hune, S. Mamone, H. Schroeder, A. P. Jagtap, S. Sternkopf, G. Stevanato, S. Korchak, C. Fokken, C. A. Muller, A. B. Schmidt, D. Becker and S. Gloggler, Metabolic Tumor Imaging with Rapidly Signal-Enhanced 1-(13) C-Pyruvate-d(3), *ChemPhysChem*, 2023, **24**, e202200615.

66 V. A. Guarino, W. M. Oldham, J. Loscalzo and Y. Y. Zhang, Reaction rate of pyruvate and hydrogen peroxide: assessing antioxidant capacity of pyruvate under biological conditions, *Sci. Rep.*, 2019, **9**, 19568.

67 A. P. Jagtap, S. Mamone and S. Gloggler, Molecular precursors to produce para-hydrogen enhanced metabolites at any field, *Magn. Reson. Chem.*, 2023, **61**, 674–680.

68 J. W. Gordon, S. B. Fain and I. J. Rowland, Effect of lanthanide ions on dynamic nuclear polarization enhancement and liquid-state T1 relaxation, *Magn. Reson. Med.*, 2012, **68**, 1949–1954.

69 E. Cavallari, C. Carrera, M. Sorge, G. Bonne, A. Muchir, S. Aime and F. Reineri, The (13)C hyperpolarized pyruvate generated by ParaHydrogen detects the response of the heart to altered metabolism in real time, *Sci. Rep.*, 2018, **8**, 8366.

70 B. J. Tickner, P. J. Rayner and S. B. Duckett, Using SABRE Hyperpolarized (13)C NMR Spectroscopy to Interrogate

Organic Transformations of Pyruvate, *Anal. Chem.*, 2020, **92**, 9095–9103.
71 R. L. Bailone, H. C. S. Fukushima, L. K. de Aguiar and R. C. Borra, Calcium Chloride Toxicology for Food Safety Assessment Using Zebrafish (Danio rerio) Embryos, *Comp. Med.*, 2022, **72**, 342–348.
72 A. L. Nelson and L. Porter, *StatPearls*, Treasure Island (FL), 2024.
73 D. J. Kushner, A. Baker and T. G. Dunstall, Pharmacological uses and perspectives of heavy water and deuterated compounds, *Can. J. Physiol. Pharmacol.*, 1999, **77**, 79–88.
74 C. Asmus, O. Mozziconacci and C. Schoneich, Low-temperature NMR characterization of reaction of sodium pyruvate with hydrogen peroxide, *J. Phys. Chem. A*, 2015, **119**, 966–977.
75 S. L. P. Gianturco, L. Laura, K. D. Storm, S. Y. Yoon, V. Melissa and A. N. Mattingly, *Hydrogen peroxide: Summary Report*, University of Maryland Center of Excellence in Regulatory Science and Innovation (M-CERSI) and University of Maryland School of Pharmacy, 2020.
76 M. Abdollahi and A. Hosseini, Hydrogen Peroxide, in *Encyclopedia of Toxicology*, ed. P. Wexler, Elsevier Inc., Academic Press, 3rd edn, 2014, vol. 2, pp. 967–970.
77 Medscape, **https://reference.medscape.com/drug/cacl-or-cacl-2-calcium-chloride-344432**.
78 N. C. I. thesaurus, Calcium Chloride (Code C28901), National Cancer Institute, 2024.
79 E. Anitua, R. Prado, M. Troya, M. Zalduendo, M. de la Fuente, A. Pino, F. Muruzabal and G. Orive, Implementation of a more physiological plasma rich in growth factor (PRGF) protocol: Anticoagulant removal and reduction in activator concentration, *Platelets*, 2016, **27**, 459–466.
80 L. P. Msezane, M. H. Katz, O. N. Gofrit, A. L. Shalhav and K. C. Zorn, Hemostatic agents and instruments in laparoscopic renal surgery, *J. Endourol.*, 2008, **22**, 403–408.
81 D. W. Lee and B. Cohan, Refractory cardiogenic shock and complete heart block after verapamil SR and metoprolol treatment. A case report, *Angiology*, 1995, **46**, 517–519.
82 K. Kawai, B. J. Larson, H. Ishise, A. L. Carre, S. Nishimoto, M. Longaker and H. P. Lorenz, Calcium-based nanoparticles accelerate skin wound healing, *PLoS One*, 2011, **6**, e27106.
83 U. Koellisch, C. Laustsen, T. S. Norlinger, J. A. Ostergaard, A. Flyvbjerg, C. V. Gringeri, M. I. Menzel, R. F. Schulte, A. Haase and H. Stodkilde-Jorgensen, Investigation of metabolic changes in STZ-induced diabetic rats with hyperpolarized [1-13C]acetate, *Physiol. Rep.*, 2015, **3**, e12474.
84 A. Flori, M. Liserani, F. Frijia, G. Giovannetti, V. Lionetti, V. Casieri, V. Positano, G. D. Aquaro, F. A. Recchia, M. F. Santarelli, L. Landini, J. H. Ardenkjaer-Larsen and L. Menichetti, Real-time cardiac metabolism assessed with hyperpolarized [1-(13) C]acetate in a large-animal model, *Contrast Media Mol. Imaging*, 2015, **10**, 194–202.
85 E. F. R. Mikkelsen, C. O. Mariager, T. Norlinger, H. Qi, R. F. Schulte, S. Jakobsen, J. Frokiaer, M. Pedersen, H. Stodkilde-Jorgensen and C. Laustsen, Hyperpolarized [1-(13)C]-acetate Renal Metabolic Clearance Rate Mapping, *Sci. Rep.*, 2017, **7**, 16002.
86 J. Steinhauser, P. Wespi, G. Kwiatkowski and S. Kozerke, Production of highly polarized [1-(13) C]acetate by rapid decarboxylation of [2-(13) C]pyruvate - application to hyperpolarized cardiac spectroscopy and imaging, *Magn. Reson. Med.*, 2019, **82**, 1140–1149.
87 V. Ruiz-Rodado, J. R. Brender, M. K. Cherukuri, M. R. Gilbert and M. Larion, Magnetic resonance spectroscopy for the study of cns malignancies, *Prog. Nucl. Magn. Reson. Spectrosc.*, 2021, **122**, 23–41.
88 C. A. Pfortmueller and E. Fleischmann, Acetate-buffered crystalloid fluids: Current knowledge, a systematic review, *J. Crit. Care*, 2016, **35**, 96–104.
89 B. Ergin, A. Kapucu, P. Guerci and C. Ince, The role of bicarbonate precursors in balanced fluids during haemorrhagic shock with and without compromised liver function, *Br. J. Anaesth.*, 2016, **117**, 521–528.
90 K. L. Ellekjaer, A. Perner, M. M. Jensen and M. H. Moller, Lactate versus acetate buffered intravenous crystalloid solutions: a scoping review, *Br. J. Anaesth.*, 2020, **125**, 693–703.
91 B. M. Mitruka and H. M. Rawnsley, *Clinical, biochemical and hematological reference values in normal experimental animals and normal humans*, Masson Publishing, New York, 1981.
92 J. E. Harkness and J. E. Wagner, *Biology and husbandry, Lea & Febiger*, Philadelphia, 1989.
93 J. N. Butler, *Carbon Dioxide Equilibria and Their Applications*, New York, 1 edn, 1991.
94 M. Grashei, P. Wodtke, J. G. Skinner, S. Suhnel, N. Setzer, T. Metzler, S. Gulde, M. Park, D. Witt, H. Mohr, C. Hundshammer, N. Strittmatter, N. S. Pellegata, K. Steiger and F. Schilling, Simultaneous magnetic resonance imaging of pH, perfusion and renal filtration using hyperpolarized (13)C-labelled Z-OMPD, *Nat. Commun.*, 2023, **14**, 5060.